Materials Science & Engineering C 91 (2018) 486–495

Syntheses of gold nanoparticles and their impact on the cell cycle of breast cancer cells subjected to megavoltage X-ray irradiation

Nikolina Hanžić[1], Anđela Horvat[1], Juraj Bibić[2], Klaus Unfried[3], Tanja Jurkin[4], Goran Dražić[5], Inga Marijanović[6], Neda Slade[1,] * and Marijan Gotić[7,] *

[1]*Laboratory for Protein Dynamics, Ruđer Bošković Institute, 10002 Zagreb, Croatia*
[2]*University Hospital Center Zagreb, Kišpatićeva 12, 10000 Zagreb, Croatia*
[3]*IUF Leibniz-Institut für Umweltmedizinische Forschung, Auf'm Hennekamp 50, 40225 Düsseldorf, Germany*
[4]*Radiation Chemistry and Dosimetry Laboratory, Ruđer Bošković Institute, 10002 Zagreb, Croatia.*
[5]*National Institute of Chemistry, Hajdrihova 19, SI-1001 Ljubljana, Slovenia*
[6]*Faculty of Science, University of Zagreb, HR 10001 Zagreb, Horvatovac102a, Croatia*
[7]*Center of Excellence for Advanced Materials and Sensing Devices, Ruđer Bošković Institute, 10002 Zagreb, Croatia*

Abstract

The gold nanoparticles (AuNPs) were synthesized in the presence of citrate (Au-CIT), glutathione (Au-GSH) and aminodextran (Au-DEX) in order to modify AuNPs surfaces and to increase their cellular uptake in the breast cancer cells MDA-MB-231. AuNPs were characterized with respect to their particle size, shape and colloidal stability in aqueous solution and cell media. The mass accumulation of each AuNP type inside cancer cells was determined quantitatively using Inductive Coupled Plasma – mass spectroscopy. The sub-cellular accumulation was studied using Transmission Electron Microscopy (TEM). It was found that gold nanoparticles applied to cancer cells localized in cytoplasmic vesicles and that the highest uptake was shown with Au-GSH nanoparticles. The effect of AuNPs on the cell cycle was investigated using flow cytometry and western blot analysis. The gold nanoparticles by themselves did not affect the cell cycle as shown by flow cytometry. Furthermore, the cancer cells were irradiated using conventional clinically relevant high-energy X-ray radiation of 6 megavolts (MV) with the dose of 4 Gy. The results on irradiated cells alone observed S phase arrest six and eight hours after irradiation and G2/M arrest 24 and 48 hours after irradiation. The irradiation of breast cancer cells treated with AuNPs has shown no significant variation in cell cycle distributions in contrast to X-ray radiation alone.

Keywords: gold nanoparticles; cancer cells; cell cycle; megavoltage radiation; MDA-MB-231; glutathione; dextran

*Corresponding authors. Tel.: +385 1 4561 111; Fax: +385 1 4561 123

E-mail addresses: gotic@irb.hr (Marijan Gotić) and Neda.Slade@irb.hr (Neda Slade)

1. Introduction

Today gold, because of its physical and chemical properties, has become an attractive material in producing gold nanoparticles (AuNPs) for biological and biomedical applications [1-3]. AuNPs are the most exploited nanoparticles in nanomedicine and biomedical applications due to their ease of synthesis, functionalization and biocompatibility. AuNPs have been used as biosensors, as immobilization matrices for enzymes and as carriers to deliver and target drugs and biomolecules to specific cell types. They have also been proposed as new contrast and radiosensitization agents [4,5]. Hainfeld et al. [4] demonstrated that EMT-6 mammary tumours implanted in mice that received an intravenous injection of 1.9 nm AuNPs could be completely eradicated in 30 days after irradiation with 250 kVp X-rays. It is believed that observed high AuNPs radiosensitization effect is due to two main reasons: *(i)* high accumulation of AuNPs in the tumour because of the leaky nature of tumour vasculature and *(ii)* high physical enhancement, because at kilovoltage (kV) photon energies the photon absorption by AuNPs (heavy metals) is much higher than by soft tissue in the body. Shi et al. [6] synthesized tiopronin-coated gold nanoparticles (Tio-AuNPs) and studied their radiosensitization effect using HCT116 human colorectal carcinoma cell line in combination with low-energy X-ray (26 keV effective energy) radiation. The relatively high radiosensitization enhancement ratios of 1.48 and 1.69 were found for HCT116 cells incubated with 0.1 mg/mL and 0.25 mg/mL of Tio-AuNPs, respectively. Antosh et al. [7] used the pH sensitive tumour-targeting agent (pH Low-Insertion Peptide) to tether 1.4-nm gold nanoparticles to cancer cells. The AuNPs modified by pHLIP tethered to the lipid bilayer of the plasma membrane. The AuNPs conjugated to pHLIP produced a statistically significant decrease in cell survival with 250 kVp X-ray radiation compared with cells without AuNPs and cells with AuNPs alone. Yasui et al. [8] reported that PEGylated nanogel containing gold nanoparticles (AuNPs) radiosensitized murine squamous cell carcinoma SCC VII and Chinese hamster lung finroblastsV79 using 200 kVp X-ray radiations. They found that GNG radiosensitized cell by enhancing apoptosis and impairing DNA repair capacity via overexpression of endoplasmic reticulum stress-related protein. However, the enhancement with commercial radiotherapy accelerators that work at megavoltage (MV) energies is very difficult to observe, because at these energies the heavy metal and soft tissue have similar absorption [3,9,10]. Jain *et al* [9] studied AuNPs radiosensitization at kV and MV photon energies. Normal epithelial cells L132, prostate cancer cells DU145, and breast cancer MDA-MB-231 cells were used. The results have shown that in MDA-MB-231 cells radiation sensitizer enhancement was achieved using 160 kVp, 6 MV, and 15 MV X-ray energies, while no significant effect was observed in L132 or DU145 cells. The MDA-MB-231 cell sensitization was observed at kV and MV photon energies. Chithrani et al. [11] showed that intracellular uptake was highly dependent upon the physical dimensions of the AuNPs. It has been shown that AuNPs of 50 nm

in diameter have the highest cellular uptake and radiosensitization enhancement factor (1.43 at 220 kVp and 1.17 at 6 MVp) compared to AuNPs of 14 and 74 nm. The functionalized gold nanoparticles with modified surface properties can be used in order to increase cellular uptake and radiation cytotoxicity in cancer cells in comparison to the normal cells. For instance, Kong et al. [12] synthesized cysteamine (Au-AET) and thioglucose (Au-Glu) modified gold nanoparticles and studied cell uptake and radiation cytotoxicity enhancement in the breast cancer cell line MCF-7. It was shown that cancer cells take up functional Au-Glu significantly more than naked AuNPs. Moreover, the results showed that surface modified AuNPs had little or no toxicity to breast cancer cells and that AuNPs significantly enhance cancer killing in comparison with irradiation alone (200 kVp X-rays). Wang et al. [13] reported that thioglucose-bound gold nanoparticles combined with megavoltage X-rays increased the radiosensitivity of MDA-MB-231 (breast cancer cells) and A549 (human lung carcinoma) cells.

In this work three types of AuNPs were synthesized in the presence of different capping and stabilizating agent, AuNPs capped with citrate (Au-CIT), glutathione (Au-GSH) and DEAE-dextran (Au-DEX) were synthesized as stable aqueous suspensions (Fig. 1, insets). GSH and DEAE-dextran were used in order to improve stability of AuNPs against aggregation in aqueous solutions and physiological conditions (Fig. 1S in Supplementary material). Besides, the selection of capping agents was of importance to modify the surface of AuNPs, such that the concentration of AuNPs inside cancer cells was optimised. The synthesis of AuNPs using citrate was introduced by Turkevich *et al* in 1951 [14] and reinvestigated by Frens in 1973 [15]. The method of synthesis uses the citrate ligand as a reducing and stabilizing agent. This method is readily duplicated with it possible to tune nanoparticle sizes from 12 to 100 nm by simply changing the Au^{3+} to citrate concentration ratio. Citrate synthesis is used by the majority of researchers and by the National Institute of Standard and Technology (NIST) to address a need identified by the cancer research community [16]; therefore the Au-CIT nanoparticles can be referred to as “reference AuNPs”. Glutathione in reduced form (GSH) is a tripeptide (γ-Glu-Cys-Gly) which consists of three amino acids: glutamic acid, cysteine, and glycine. Thus, it contains a thiole bond, a carboxyl acid group and amino group. It is a water soluble and biocompatible molecule, which uses its strong thiole bond to stabilize AuNPs. Moreover, due to the presence of carboxyl acid and the amino group, the solution pH determines the AuNPs size (lower pH ~ larger glutathione modified AuNPs, [17]). In this work, the solution pH was adjusted to 7.0, which is near physiological pH. Zhou *et al* [18] found that glutathione has advantages over cysteine in enhancing the stability of AuNPs under physiological conditions. Despite its abundance in the cytoplasm, it has a low affinity to cellular proteins. Recent study showed that even very small (2.5 nm) glutathione-coated AuNPs owned long tumour retention and fast normal tissue clearance [19]. DEAE-dextran (Diethylaminoethyl-dextran hydrochloride) is a robust cationic polymer (positively charged at all pH values), which improves stability at high AuNPs concentration and causes production of better

dispersed AuNPs with narrow size distribution. It has been successfully used for the synthesis and stabilization of cadmium sulphide [20] and gold nanoparticles [21]. DEAE-dextran is hydrophilic polymer with amino groups that are free for additional functionalization. It is highly biocompatible material with the application in biomedicine such as adjuvant in vaccines, transfection agent and stabilizer of proteins. Cancer cells have much faster metabolism than normal cells, which leads to the higher rate of uptake of materials needed for the cell's survival (such as polysaccharides). Therefore, in this work the DEAE-dextran (aminodextran) was used to synthesize well-dispersed and highly concentrated gold colloidal suspension and to increase the concentration of AuNPs in cancer cells.

The synthesized AuNPs were applied to a breast cancer cell line MDA-MB-231 and their subcellular and quantitative mass accumulations inside cancer cells were investigated. It is well known that the high accumulation of AuNPs inside the cancer cells is one of the major prerequisites for radiation cytotoxicity enhancement [3,4,9-13,22,23]. The cancer cells were irradiated using conventional clinically relevant high-energy X-ray radiation of 6 MV. The impact of AuNPs on the cell cycle was studied using flow-cytometry and Western blot analysis. The cell cycle effects of synthesized AuNPs applied to breast cancer cells after exposure to the 6 MV X-ray radiation were studied.

2. Materials and Methods

2.1. Reagents

Tetrachloroauric acid ($HAuCl_4 \times 3H_20$, Alfa Aeser GmbH & Co KG, Germany), sodium citrate dihydrate ($C_6H_5Na_3O_7$, Kemika, Croatia), sodium borohydride ($NaBH_4$, Sigma Aldrich, USA), γ-L-Glutamyl-L-cysteinyl-glycine (GSH, $C_{10}H_{17}N_3O_6S$; Sigma Aldrich, USA) and Diethylaminoethyl-dextran hydrochloride (DEAE-dextran, Sigma Aldrich, USA), were used as received.

2.2. Synthesis of gold nanoparticles

Au-CIT were synthesized using the classical Turkevich method [14]. Briefly, 102.5 μL aqueous solution of 4% $HAuCl_4 \times 3H_2O$ was added to deionized water (10 mL), which was heated to boiling. Aqueous solution of 1% sodium citrate (848.4 μL) was then added to the boiling solution, at which point the solution turned from clear yellow to a deep wine red. After cooling, the ruby red gold colloidal solution was filtered through a 0.22-μm filter (Spritzen-Syringe Filter, membrane: PES) and stored at 4°C.

Au-GSH were synthesized with minor modifications according to the procedure described by Brinas et al. [17]. An aqueous solution of 4% $HAuCl_4 \times 3H_2O$ (246 μL) was mixed with an aqueous solution of 19 mM GSH (7.8 mL). The pH of the resulting mixture was adjusted to 7.0 using 1 M

NaOH. A freshly prepared aqueous solution of 50 mM $NaBH_4$ (4.98 mL) was added dropwise while stirring. The mixture was allowed to react overnight at room temperature, filtered through a 0.22-µm filter (Spritzen-Syringe Filter, membrane: PES) and stored at 4°C.

Au-DEX were synthesized with minor modifications according to the procedure described by Morrow et al. [21]. An aqueous solution of 4% $HAuCl_4 \times 3H_2O$ (197 µL) was added to 10 mL of deionized water maintained at 50°C. The pH of the gold solution was adjusted to 12.0 with 10 M NaOH. An aqueous solution of 92 µM aminodextran (1 mL) was poured rapidly into the reaction vessel while stirring. The mixture was continuously maintained at 50°C for the next 8h. Once all gold was reduced, the solution was heated at 84°C for the next 4h to decompose an excess of aminodextran. After the decomposition of the aminodextran, the gold suspension was centrifuged 2 times (7000 ×g/20 min) and the supernatant solution was decanted. The precipitate was resuspended in deionized water and the resulting solution was filtered through a 0.22-µm filter (Spritzen-Syringe Filter, membrane: PES) and stored at 4°C.

2.3. Instrumental techniques

The Au-CIT, Au-GSH or Au-DEX sample suspensions were diluted in MQ-H_2O and the droplet of each sample was placed on a grid and left overnight to dry properly. Nanoparticle shape and size was determined using Transmission Electron Microscope (TEM, Jeol 1400, Japan). ImageJ (version 1.50a) computer program was used to measure the nanoparticle size. Optical absorption spectra of AuNP suspension in the wavelength range of 200-800 nm was measured by UV-Visible spectrometer (UV-3600, Shimadzu, Japan). The size, hydrodynamic diameter and zeta-potential of Au-NPs colloidal suspension in MQ-H2O and in growth media were determined using Dynamic Light Scattering (Zetasizer Nano S, Malvern Instruments Ltd, UK).

2.4. Cell line

MDA-MB-231 breast cancer cells (ATCC ® HTB-26 ™) were maintained in DMEM medium (Sigma Aldrich, USA), supplemented with 10% FBS (Life Technologies, USA), 1% penicillin-streptomycin (Sigma Aldrich, USA), 1% L-glutamine (Sigma Aldrich, USA) and 1% sodium pyruvate (Life Technologies, USA), in a humidified incubator at 37°C with 5 % CO_2. Cell line was tested free of mycoplasma contamination.

2.5. MTT cell viability assay

A total of 3.5 x 10^3 cells/well were plated into 96-well tissue culture dishes for 24 h, then exposed to increasing concentrations of Au-CIT, Au-GSH and Au-DEX nanoparticles (10-100 µM) for further 48 h. After exposure, cells were treated with MTT (3-(4, 5-dimethylthiazol- 2-yl)-2, 5-diphenyltetrazolium bromide) solution (Sigma Aldrich, USA) in concentration of 20 µg/40 µl. After for 3 h of incubation at 37°C DMSO was added to each well to dissolve the precipitates and the

absorbance was measured on microplate reader at 570 nm. All assays were performed in quadruplicates in three individual experiments. The cell viability was expressed as percentage of absorbance after the treatment with different concentrations of AuNPs in comparison to the absorbance without the treatment.

2.6. Cellular uptake of gold nanoparticles

A total of 1.7 x 10^5 cells were plated in 60 mm tissue culture dishes a day before the exposure to Au-CIT, Au-GSH or Au-DEX nanoparticles. After 24 h of incubation cells were washed twice in phosphate-buffered saline (PBS), trypsinized, pelleted, fixed in 2% gluteraldehyde in cacodylate buffer for 4h, which was replaced with cacodylate buffer overnight. After fixation in 1% agar solution samples were cut into small cubes (approximately $1mm^3$) and fixed with 1% osmium tetroxide in the cacodylate buffer, dehydrated sequentially with 50%, 60%, 70%, 80% and 96% ethanol and embedded in the Spurr resin. The polymerized blocks were dissected, the ultrathin sections were placed on cooper grids and investigated using transmission electron microscope (JEOL 1400).

2.7. Inductively coupled plasma–mass spectroscopy

A total of 1.7 x 10^5 cells were plated in 60 mm tissue culture dishes and incubated for 24 h, then exposed to Au-CIT, Au-GSH or Au-DEX for further 48 h, washed ten times in PBS, trypsinized, counted and digested in *aqua regia* (nitric acid : hydrochloric acid= 1:3). Gold mass in each solution was measured using Inductive Coupled Plasma – mass spectrometry (ELEMENT 2™ ICP MS, TermoFisfer Scientific, USA). The number of AuNPs was calculated via the gold mass, and the number of AuNPs in the solution was divided by the number of cells to yield the average number of AuNPs taken up per cell.

2.8. Protein extraction

A total of 5 x 10^5 cells were plated in 100 mm tissue culture dishes and incubated for 24 h, exposed to Au-CIT, Au-GSH or Au-DEX nanoparticlesfor for 48 h before irradiation. Irradiation was performed using clinical linear accelerator (Siemens Primus, Germany). Mega-voltage radiation (6 MV) was delivered at total dose of 4 Gy with a dose rate of 4 Gy/ min. After irradiation, cells were incubated at 37°C with 5% CO_2 for further 6 and 24 h. After incubation, cells were lysed with 0.1% NP40 buffer (50 mMTris, 10% glycerol, 0.1% NP-40, 100 mMNaCl, 0.2 mM EDTA) in combination with vanadate (1:1000) and protein inhibitors (Complete, Mini, EDTA-free; Roche Diagnostics, USA). Lysates were incubated on ice and centrifuged (5000 rpm; 4°C; 7 min). Supernatants were collected and protein concentration was determined with Pierce™BCA Protein Assay Kit (Termo Fisher Scientific, USA).

2.9. Gel electrophoresis and immunobloting

The 30 μg of lysate was initially denatured in 4 × Loading Buffer (40% glycerol, 240 mM Tris-HCl pH 6.8, 8% SDS, 0.04% bromophenol blue, 5% β-mercaptoethanol) at 96°C for 5 min and separated on 8%, 10% or 12% SDS-polyacrylamide gels and transferred to nitrocellulose membranes (Whatman Protran BA 83; 0.2 μm pores) and blocked with 4% skimmed milk in a TBS-Tween buffer (TBST) for 20 min. Primary antibodies in this study are as follows: mouse anti-cyclin A (Novocastra, UK), mouse anti-cyclin B1 (Santa Cruz Biotechnology, USA), rabbit anti-cyclin D1 (Santa Cruz Biotechnology, USA), mouse anti-cyclin E1 (Santa Cruz Biotechnology, USA), mouse anti-p53 DO1 (Santa Cruz Biotechnology, USA). After incubation with appropriate horseradish peroxidase-conjugated secondary antibody, proteins were visualized by using Western Lightning Plus-ECL Enhanced Chemiluminiscence Substrate (Perkin Elmer, USA). Western blots were imaged using an Alliance 4.7 imaging system (UVitec, UK).

2.10. Flow cytometry

A total of 5 x 10^5 cells were plated in 100 mm tissue culture dishes and incubated for 24 h, exposed to Au-CIT, Au-GSH or Au-DEX nanoparticles for 48 h before irradiation. After irradiation, as described below, cells were incubated for 6 and 24 hours, then trypsinized, centrifuged, fixed in 70% ethanol and stored overnight at 4°C. Before analysing, cells were resuspended in PBS with 0,1 μg/mL RNase (Sigma-Aldrich, Germany) followed by staining with 40 μg/mL propidium iodide (Molecular Probes, Eugene, OR, USA) for 30 minutes at 37°C in the dark. Analysis was performed using BD FACSCalibur™ Flow Cytometer (BD Biosciences, Ontario, Canada) and BD CELLQuest™Pro software (BD Biosciences, Ontario, Canada). The data were analysed by FlowJo software (Flow Cytometry Analysis Software, USA). Values were expressed as fractions of cells in cell cycle phases (the mean ± standard deviation). Each experiment was performed three times.

2.11. Irradiation setup

Megavoltage X-ray (6 MV) irradiation was performed using a clinical linear accelerator (SiemensPrimus, Germany) with a dosimetric calibration. Source-to-surface distance (SSD) was 100 cm and field size was 15 × 15 cm^2. Three centimeters of a Plexiglass sheet (water-equivalent slabs phantom) was placed on the bottom and on the top of the dishes containing the cells to serve as a built-up material for the 6 MV beam. Mega-voltage radiation (6 MV) was delivered at total dose of 4 Gy with a dose rate of 4 Gy/min^-. *In vivo* radiation diode dosimetry measurements were performed for beam calibration and variation within a field smaller than 1% for each well.

2.12. Statistical analysis

The one-way analysis of variance (ANOVA) and Tukey *HSD*multiple comparison tests were used. Differences less than 0.05 ($p< 0.05$) were considered statistically significant.

3. Results and discussion

3.1. Characterization of synthesized gold nanoparticles

Fig. 1 shows UV-vis spectra and images of synthesized samples. The position, width and intensity of surface plasmon resonance (SPR) band depend on gold nanoparticle size, shape, concentration and interparticle interactions. The SPR band has been regularly used for the determination of particle size. In this work the size of AuNPs was calculated using the procedure presented by Haiss et al. [24]. The results of UV-Vis characterisations of AuNP samples are given in Table 1.

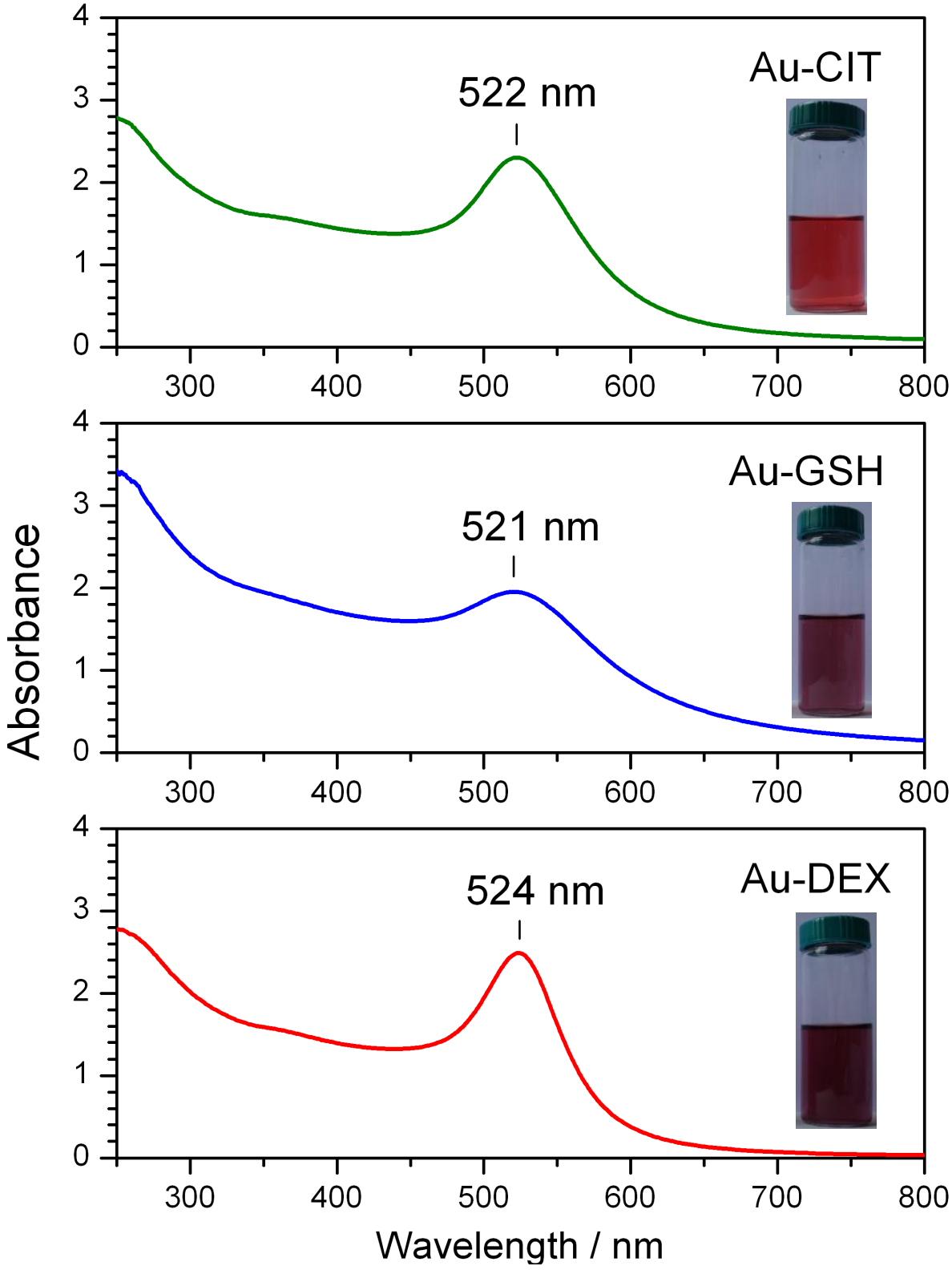

Fig. 1 UV-Vis spectra and images of samples Au-CIT, Au-GSH and Au-DEX.

Table 1 Diameters (*D*) of synthesized gold nanoparticles measured using UV-Vis, TEM and DLS techniques.

SAMPLES	λ_{SPR} (nm)	$D_{(UV\text{-}Vis)}$**	$D_{(TEM)}$	$D_{(DLS)}$
Au-CIT	522	17.0 nm	16.4 nm	47.0 nm
Au-GSH	521	4.0 nm	8.8 nm	11.0 nm
Au-DEX	524	30.0 nm	21.9 nm	200.0 nm

* λ_{SPR} = the position of Surface Plasmon Resonance peak in UV-Vis spectra

** Diameter (*D*) of AuNPs was calculated using the procedure presented by Haiss et al. (2007).

The hydrodynamic diameter (Fig. 2 and Table 1) and zeta-potential (ξ-potential) of AuNPs sample suspensions in MQ-H_2O and in growth media were determined using Dynamic Light Scattering. In the aqueous solution, ξ-potential of AuNPs is high and it ensures colloidal stability for the Au-CIT (ξ-potential = -52 mV), the Au-GSH (ξ-potential = - 49,6 mV) and the Au-DEX (ξ-potential = + 40,2 mV) nanoparticles over several weeks. The positive ξ-potential of sample Au-DEX is due to the presence of protonated amino groups. The DLS technique, unlike TEM and UV VIS, which measure the diameter of gold core, measures the hydrodynamic diameter of gold nanoparticles. The hydrodynamic diameter of sample Au-DEX includes the polymer and solvent (hydration) layer on the surface of gold core that moves all together under the influence of Brownian motion. Thus, the high discrepancy between the Au-DEX gold diameters determined using UV-Vis (30.0 nm) and TEM (21.9 nm) with the hydrodynamic diameter of Au-DEX determined using DLS (200.0 nm) are due to the robust cationic DEAE-dextran polymer that behaves like surfactant and at relative high concentration significantly contributes to the gold hydrodynamic diameters in the sample Au-DEX. The samples Au-CIT and Au-GSH consist of small organic molecules and the hydrodynamic diameters of these samples are more comparable with UV-VIS and TEM measurements (Table 1).

The stability of samples in highly ionic medium was investigated in the concentrated NaCl solutions between 0 and 150 mM (Fig. S1 in Supplementary Info). The Au-CIT nanoparticles aggregate when the concentration of NaCl exceeds 100 mM, which is observed by changing the colour of solution from red to blue. On the other hand, the Au-DEX and Au-GSH nanoparticles retain their initial red colour over the whole range of investigated NaCl concentrations (Fig. S1) thus confirming the stability of Au-GSH and Au-DEX samples in medium of high ionic strength.

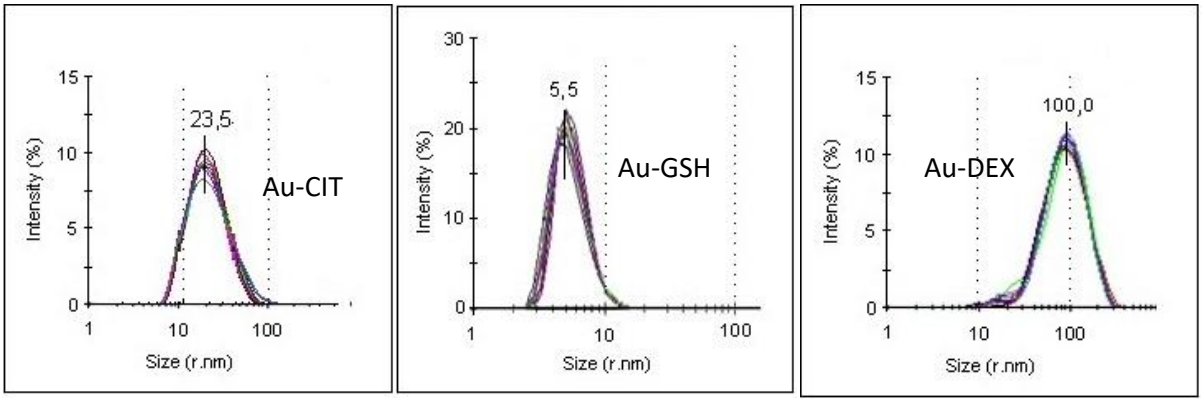

Fig. 2 The hydrodynamic radius (*r*) of synthesized sample suspensions measured using DLS. The hydrodynamic diameters (2*r*) of 47 nm, 11 nm and 200 nm in size were measured for samples Au-CIT, Au-GSH and Au-DEX, respectively.

Fig. 3 shows TEM images and corresponding particle size distributions of samples Au-CIT (a), Au-GSH (b) and Au-DEX (c). The size of nanoparticles (Table 1) was determined by analysis of approximately 200 nanoparticles using "ImageJ" computer program. Fig. 3d shows the high resolution TEM images of Au-GSH sample showing the directly measurable organic shell of approximately 2 nm in size that surrounds the nanoparticles.

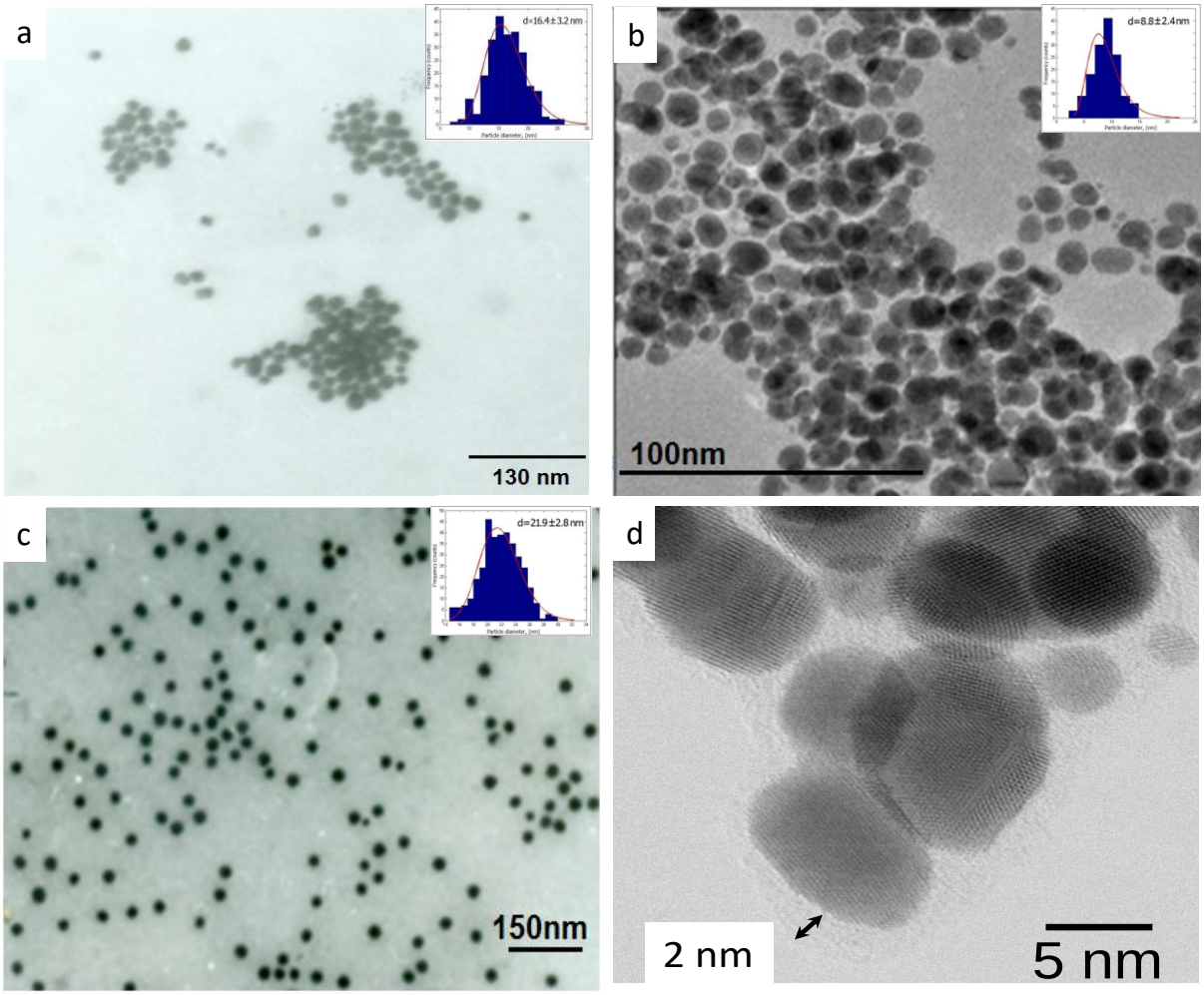

Fig. 3 TEM images of samples Au-CIT (a), Au-GSH (b) and Au-DEX (c). The corresponding particle size distributions fitted with LogNormal function are given in insets. The size of nanoparticles was determined by analysis of approximately 200 nanoparticles using "ImageJ" computer program (*d* corresponds to mean particle diameter). High resolution TEM images of sample Au-GSH showing the directly measurable organic shell of approximately 2 nm in size that surrounds the nanoparticles (d).

3.2. Subcellular internalization of AuNPs

The subcellular internalization of AuNPs in the MDA-MB-231 cells was analyzed using TEM. Nanoparticles appear to be aggregated in cytoplasmic vesicles (Fig 4a-c). Fig. 4a shows a cell with cytoplasmic vesicles. Using higher magnification (Fig 4a inset) it was observed that the vesicles contain interwoven dark matter. This high-electron dense material belongs to internalized Au-CIT nanoparticles inside the vesicles. Fig. 4b shows vesicles with Au-GSH nanoparticles, while Fig 4c

shows vesicles with Au-DEX nanoparticles. The amount of nanoparticle's uptake per cell was determined using ICP-MS (Fig 4d). The Au-GSH sample shows the highest, while the Au-CIT and Au-DEX showed lower uptake of AuNPs as calculated on the basis of number of AuNPs per cell.

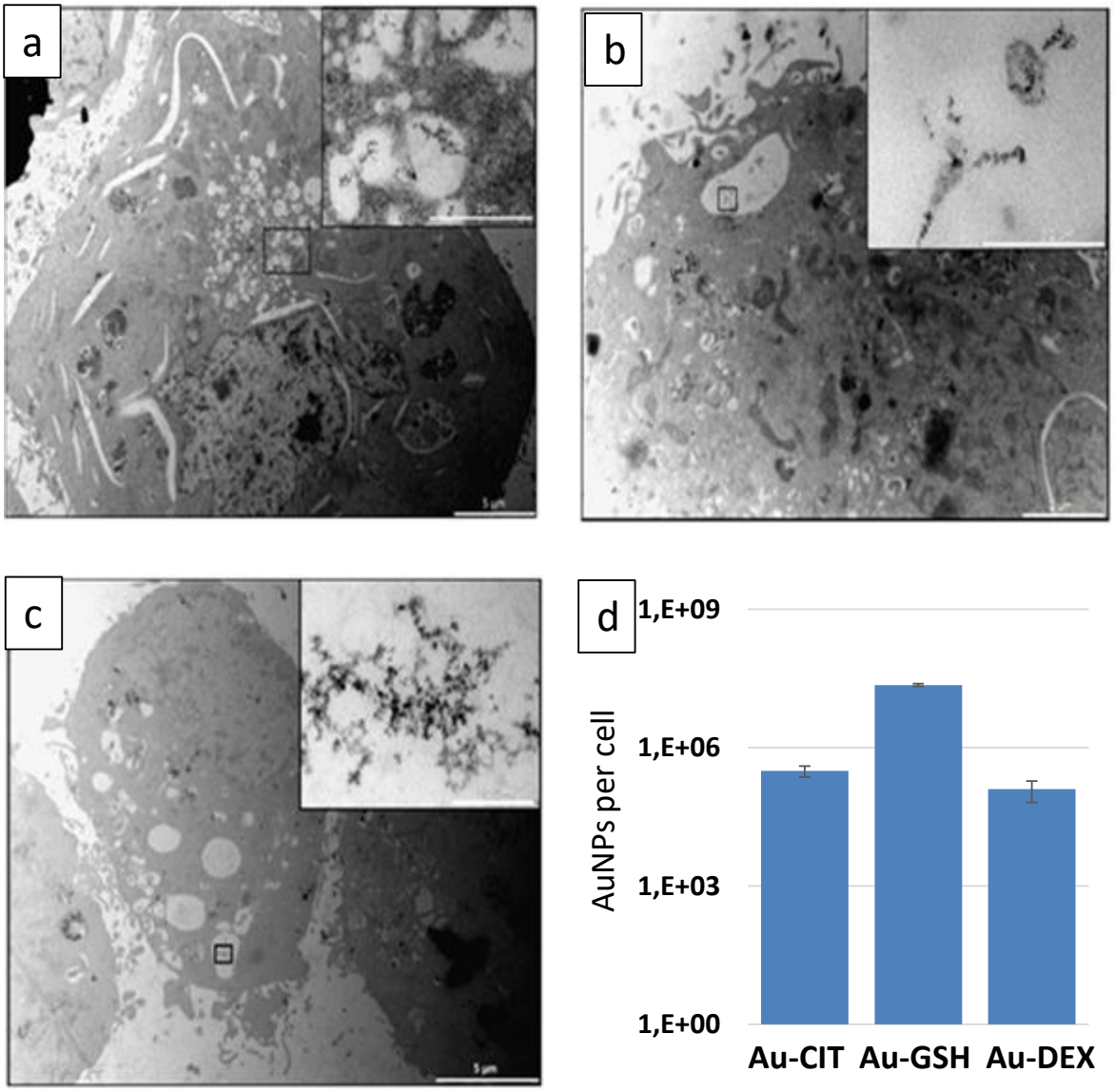

Fig. 4 Internalization of nanoparticles in MDA-MB-231 cells analysed using TEM. (a) MDA-MB-231 cells with internalized Au-CIT nanoparticles; (b) Au-GSH nanoparticles; and (c) Au-DEX nanoparticles. Nanoparticles appear to be aggregated in cytoplasmic vesicles. The amount of nanoparticle's uptake per cell was determined using ICP-MS (d). The highest uptake was observed with Au-GSH nanoparticles.

3.3. Cell viability

To determine the the effect of AuNPs concentration on cell viability, MTT test was performed. The reduction in cell viability below 80 % (IC80) was observed at concentrations of 30 μM for Au-GSH and 50 μM for both Au-CIT and Au-DEX. The cytotoxicity of AuNPs alone to cancer cells should be low, so that the effect of radiation (AuNPs + irradiations) should be as high as possible. Thus, in the radiation experiments the cells were treated with AuNPs concentrations of up to 50 μM.

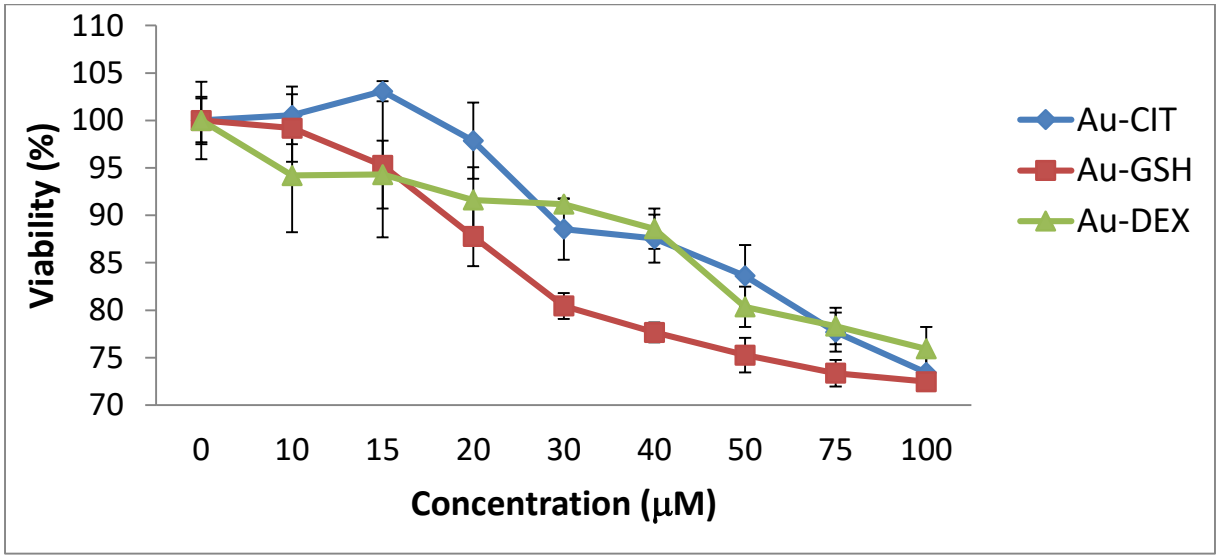

Fig. 5 MTT viability assay. MDA-MB-231 cells were treated with increasing concentrations of AuNPs for 48 h followed by determination of cell viability. Data are means ± SDs (n=4, P<0,05).

3.4. Influence of AuNPs alone on cell cycle

To find out whether the AuNPs interfere with the cell cycle, flow cytometry analysis was performed. We observed that there is no influence of nanoparticles on the cell cycle comparing to untreated control sample (Fig 6a-d). Percentage of cells in particular phase of cell cycle was uniform in all treatments (Fig 6e). Also, the regulators of cell cycle, the cyclins, determined by western blot analysis haven't shwn any change (Fig 6f).

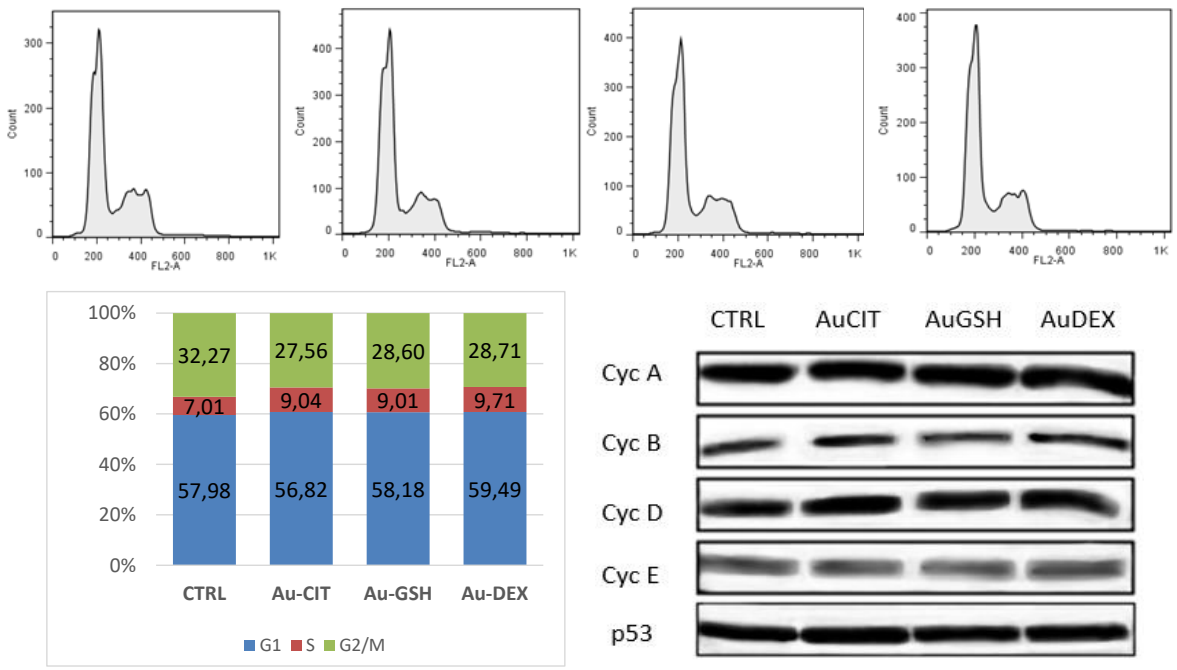

Fig. 6 The influence of synthesized AuNPs alone on cell cycle. Flow cytometry analysis shows no influence of AuNPs on the cell cycle; control untreated sample (a), AuCIT (b); AuGSH (c); AuDEX (d). Percentage of cells in particular phase of cell cycle was relatively uniform in all treatments (e).Western blot analysis (f) shows no change in the amount of the cyclins,the regulators of cell cycle. All experiments were performed in triplicates.

3.5. Influence of 6 MV radiation alone on cell cycle

MDA-MB-231 cells were irradiated with a dose of 4 Gy using clinically relevant high-energy X-ray radiation of 6 MV, collected after 2, 4, 6, 8, 24 and 48 hours and analyzed. Flow cytometry analysis observed almost no change in cell cycle progression 2 and 4 hours after irradiation. Six and eight hours after irradiation S phase arrest was observed, while 24 and 48 hours after irradiation G2/M arrest was observed (Fig 7.) Therefore, for the experiments that followed time points 6 and 24 hours after irradiation were used.

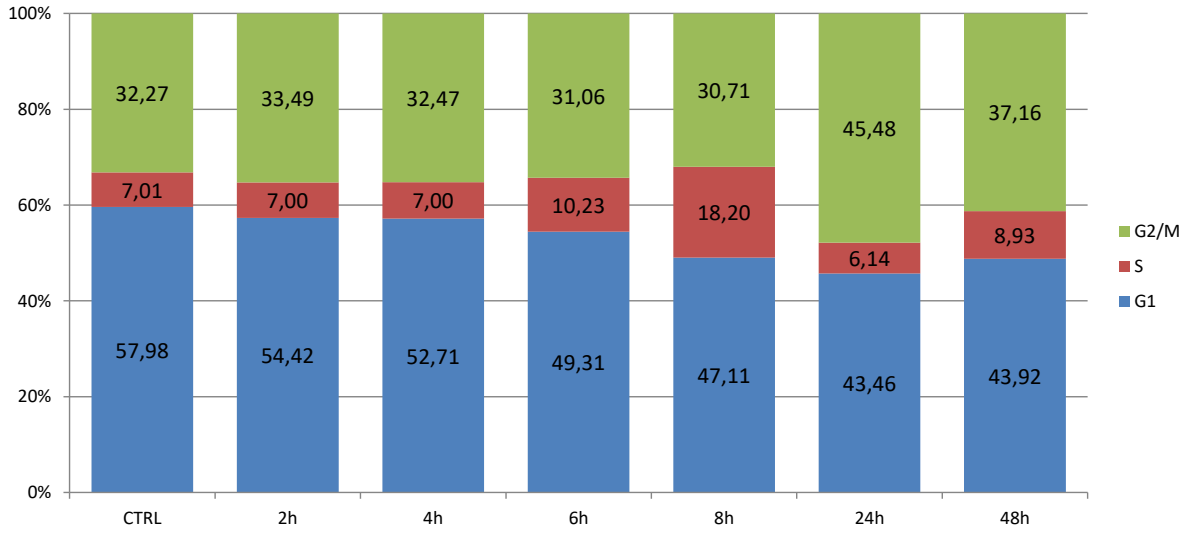

Fig. 7 Flow cytometry analysis showing the influence of 6 MV radiation on cell cycle. MDA-MB-231 cells were irradiated using clinically relevant high-energy X-ray radiation of 6 MV with a dose of 4 Gy and then collected after 2, 4, 6, 8, 24 and 48 hours and analyzed. Flow cytometry analysis observed almost no change in cell cycle progression 2 and 4 hours after irradiation. Six and eight hours after irradiation S phase arrest was observed, whereas 24 and 48 hours after irradiation G2/M arrest was observed. All experiments were performed in triplicates.

Fig. 8a-c shows flow cytometry analysis 6 and 24 hours after irradiation. The S phase and G2/M phase arrest are clearly visible. Fig. 8d shows the percentage of cells in particular phase of cell cycle. Western blot analysis showed accumulation of cyclin B and cyclin D six and 24 hours after irradiation. Also, p53 was overexpressed 24 h after irradiation (Fig 8e).

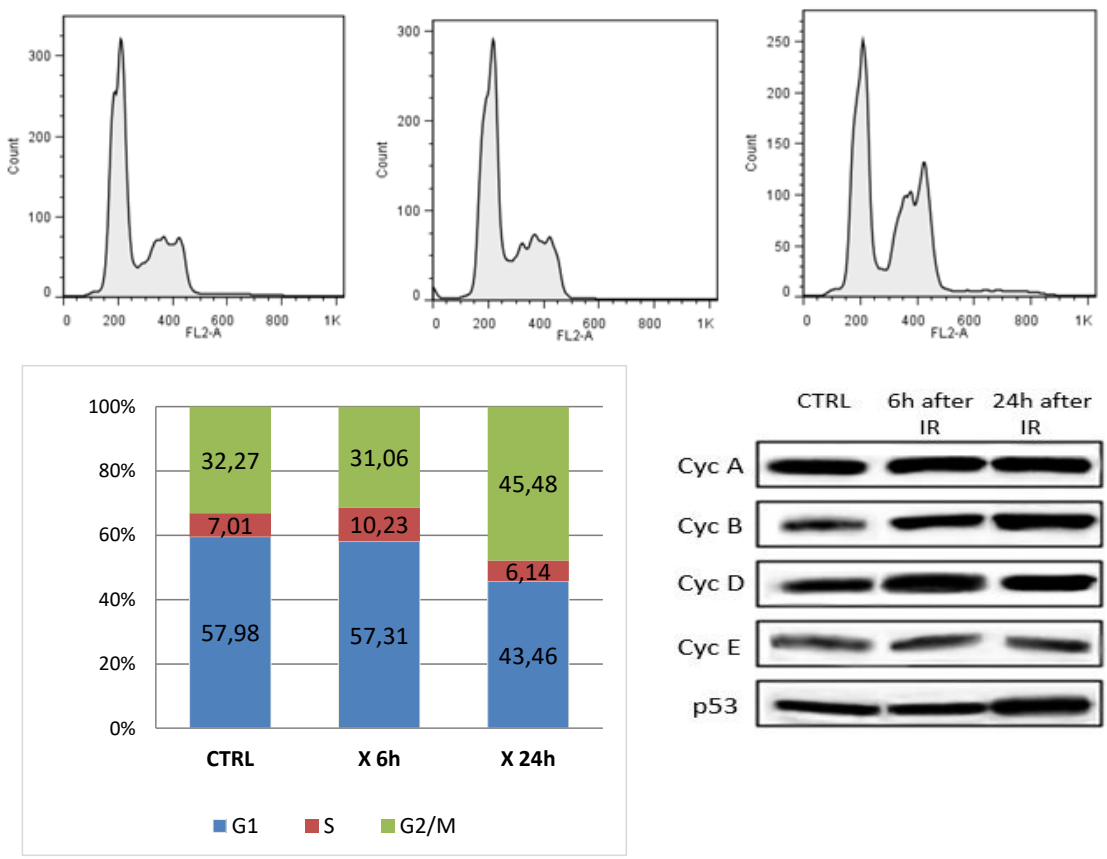

Fig. 8 The influence of 6 MV radiation alone on cell cycle. Flow cytometry analysis shows mild S phase arrest in cell cycle progression 6 h after irradiation, while 24 h after irradiation G2/M arrest was observed: control untreated sample (a); 6 h after irradiation (b); 24 h after irradiation (c). The percentage of cells in particular phase of cell cycle (d). Western blot analysis (e) shows accumulation of cyclin B and cyclin D six and 24 hours after irradiation. Besides, p53, was overexpressed 24 h after irradiation. All experiments were performed in triplicates.

3.6. Influence of AuNPs + 6 MV X-ray radiation on cell cycle

In order to study the biological effect of AuNPs + irradiation on the MDA-MB-231 cancer cells, flow cytometry analysis was performed. Six hours after irradiation, at the beginning of S phase arrest, there was no change in cell cycle distribution between the samples pretreated with Au-CIT, Au-DEX or Au-GSH in contrast to irradiated control cells (Fig 9a-left). Twenty four hours after irradiation, all samples showed similar G2/M arrest (Fig 9a - right). Western blot analysis showed mild accumulation of cyclin D six hours after irradiation as well as accumulation of cyclin B and p53 twenty four hours after irradiation in all samples (Fig 9b).

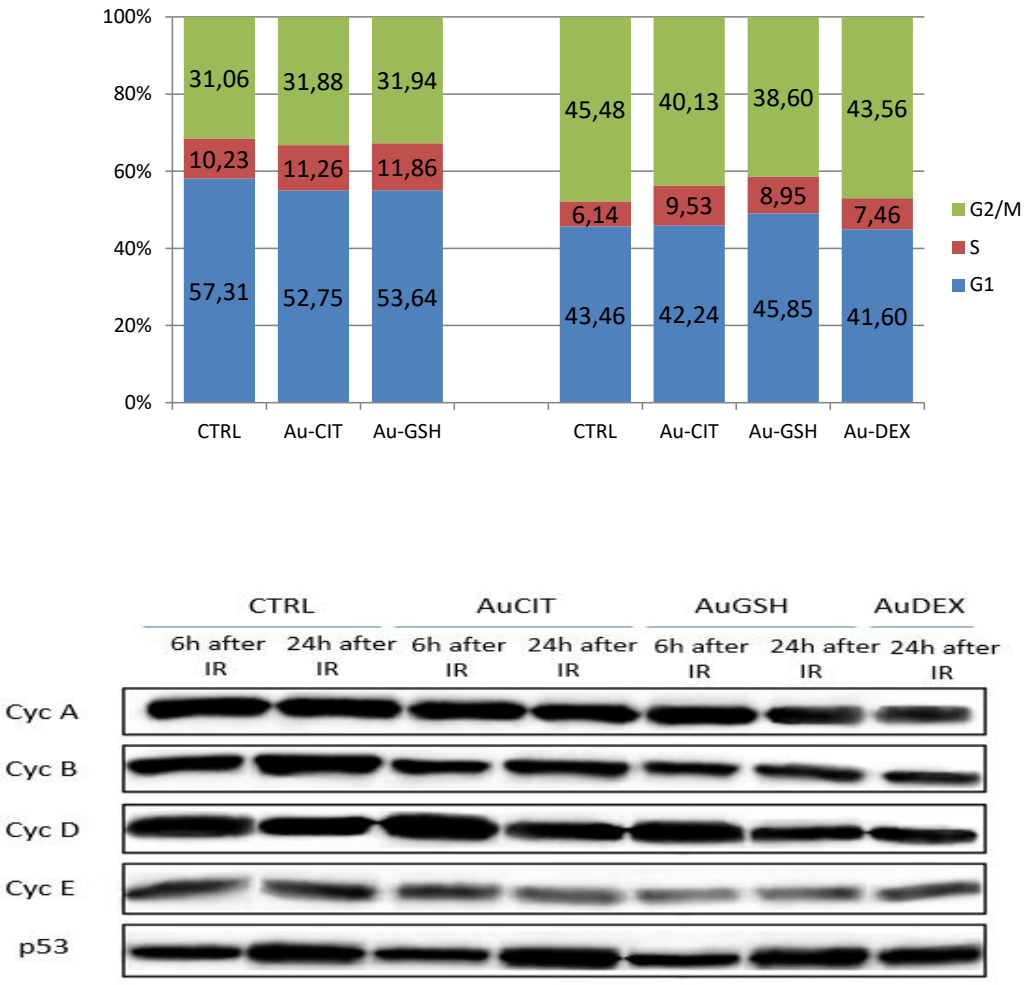

Fig. 9 The influence of AuNPs + 6 MV X-ray radiation on cell cycle. Flow cytometry analysis shows almost no change in cell cycle distribution upon irradiation between the samples pretreated with Au-CIT, Au-GSH or Au-DEX. Six hours after irradiation there was no change in cell cycle distribution and 24 h after irradiation all samples showed similar G2/M arrest (a). Western blot analysis (b) showed mild accumulation of cyclin D six hours after irradiation, as well as accumulation of cyclin B and p53 24 hs after irradiation in all samples. All experiments were performed in triplicates.

The regulation of the cell cycle is a very important determinant of the sensitivity to ionizing radiation [25-27]. The AuNPs alone can induce alterations in cell cycle distribution [3,27]. However, in this work we have found no interference of synthesized AuNPs alone on cell cycle (Fig. 6). This finding is in line with published reports by Pan et al. [28] and Cui et al. [29]. On the other hand, the irradiation (6 MV X-ray) alone caused S phase and G2/M phase arrest (Fig. 8d). Western blot analysis showed accumulation of cyclin B and cyclin D six and 24 hours after irradiation. Besides, protein p53 [30], was overexpressed 24 h after irradiation (Fig 8e). However, the irradiation of breast cancer cells treated with AuNPs has shown no significant variation in cell cycle distributions compared to X-ray radiation alone. There are very few studies dealing with the impact of AuNPs on the cell cycle after irradiation [3]. In one study Roa et al. [31] synthesized glucose-capped AuNPs (Glu-AuNPs) in order to improve cellular uptake and radiosensitization in radiation-resistant human prostate cancer DU145 cells. They investigated the effect of Glu-AuNPs on cell cycle regulation and on radiosensitivity and have found that Glu-AuNPs induced acceleration in the G0/G1 phase and accumulated DU145 cells in the G2/M phase via the activation of the CDK kinases. Also, G2/M arrest was accompanied by decreased expression of p53 and cyclin A and increased expression of cyclin B1 and cycline E. Coulter et al. [32] studied the uptake, localization and cytotoxicity of 1.9 nm AuNPs to cancer and normal cells. The immortalized normal cell line did not endocytose AuNPs as efficiently as the tumour cell lines andAuNPs were mostly endocytosed and localized within citoplasmic vesicles. The AuNPs induced an increased production of reactive oxygen species and this correlated with increased cytotoxicity. Xu et al [33] synthesized gold nanorods (AuNRs) conjugated with arginine (R)-glycine (G)-aspartate (D) (RGD) peptides in order to sensitize melanoma A375 cells to irradiation. They showed that RGD-AuNRs are readily incorporated into melanoma cells through integrin $\alpha_v\beta_3$ – receptor-mediated endoycytosis. The RGD-AuNRs plus X-ray irradiation enhanced the radiosensitivity and radiation induced apoptosis and induced significant G2/M phase arrest in melanoma cells. However, in contrast to reports of other studies we observed no signs of increased sensitivity of AuNPs + 6 MV X-ray radiation on MDA-MB-231 breast cancer cells, determined at the level of cell cycle changes (Fig. 9).

4. Conclusions

Three types of AuNPs with different surface capping agents were synthesized. The surfaces of AuNPs were modified with citrate (Au-CIT), glutathione (Au-GSH) and diethylaminoethyl-dextran hydrochloride polymer (Au-DEX) in order to increase the AuNPs uptake inside cancer cells. Thus synthesized AuNPs were applied to a breast cancer cell line MDA-MB-231 and localized in cytoplasmic vesicles (Fig.5a-c). The highest uptake was shown for Au-GSH nanoparticles (Fig.5d).

Flow cytometry and western blot analysis has shown that gold nanoparticles by itself did not affect the cell cycle (Fig 6.) Further, the experiments with radiation were performed by irradiating the cancer cells using conventional clinically relevant high-energy X-ray radiation of 6 MV with the dose of 4 Gy. Flow-cytometry analysis observed S phase arrest six and eight hours after irradiation and G2/M arrest 24 and 48 hours after irradiation (Fig 7 and 8). Flow cytometry and western blot analysis have shown no change in cell cycle distribution between the samples pretreated with AuNPs in contrast to irradiated cells only (Fig 9). Thus, the synthesized AuNPs + 6 MV irradiation have shown no additional cell cycle effects in comparison to the irradiation alone.

Acknowledgments

The authors thank dipl. ing. Anamarija Bauer-Šegvić for TEM measurements, dr. Tea Mihelj for Dynamic Light Scattering measurements, dipl. ing. Lucija Horvat for help in the preparation of the ultrathin sections for TEM measurements, dr. Nevenka Mikac for Inductive Coupled Plasma – mass spectroscopy measurements and Mr. Jasmin Forić for help in experimental work. We thank dr Siniša Ivanković for valuable discussion concerning the interpretation of the results obtained in this study. The financial support of the Centre of Excellence for Advanced Materials and Sensors, "Ruđer Bošković" Institute, Croatia, is gratefully acknowledged. Neda Slade acknowledges the financial support of the Croatian Science Foundation through grant IP-11-2013-1615. Goran Dražić acknowledges the financial support of the Slovenian Research Agency (ARRS) through Program No. P2-0393 and Project J2-6754.

Compliance with Ethical Standards

Conflict of Interest: The authors declare that they have no conflict of interest.

References

[1] C.J. Murphy, A.M. Gole, J.W. Stone, P.N. Sisco, A.M. Alkilany, E.C. Goldsmith, S.C. Baxter, Gold Nanoparticles in Biology: Beyond Toxicity to Cellular Imaging, Acc. Chem. Res. 41 (12) (2008) 1721–1730. doi:10.1021/ar800035u.

[2] L. Dykman, N. Khlebtsov, Gold nanoparticles in biomedical applications: recent advances and perspectives, Chem. Soc. Rev. 41 (2012) 2256–2282. doi:10.1039/C1CS15166E.

[3] S. Rosa, C. Connolly, G. Schettino, K.T. Butterworth, K.M. Prise, Biological mechanisms of gold nanoparticle radiosensitization, Cancer Nano (2017) 8:2. doi:10.1186/s12645-017-0026-0.

[4] J.F. Hainfeld, D.N. Slatkin, H.M. Smilowitz, The use of gold nanoparticles to enhance radiotherapy in mice, Phys. Med. Biol. 49 (2004) N309–N315. doi:10.1088/0031-9155/49/18/N03.

[5] J.F. Hainfeld, D.N. Slatkin, T.M. Focella, H.M. Smilowitz, Gold nanoparticles: a new X-ray contrast agent, Br. J. Radiol. 79 (2006) 248–253. doi:10.1259/bjr/13169882.

[6] M. Shi, B. Paquette, T. Thippayamontri, L. Gendron, B. Guerin, L. Sanche, Increased radiosensitivity of colorectal tumors with intra-tumoral injection of low dose of gold nanoparticles, International Journal of Nanomedicine. Volume 11 (2016) 5323–5333. doi:10.2147/IJN.S97541.

[7] M.P. Antosh, D.D. Wijesinghe, S. Shrestha, R. Lanou, Y.H. Huang, T. Hasselbacher, D. Fox, N. Neretti, S. Sun, N. Katenka, L.N. Cooper, O.A. Andreev, Y.K. Reshetnyak, Enhancement of radiation effect on cancer cells by gold-pHLIP, Proceedings of the National Academy of Sciences. 112 (2015) 5372–5376. doi:10.1073/pnas.1501628112.

[8] H. Yasui, R. Takeuchi, M. Nagane, S. Meike, Y. Nakamura, T. Yamamori, Y. Ikenaka, Y. Kon, H. Murotani, M. Oishi, Y. Nagasaki, O. Inanami, Radiosensitization of tumor cells through endoplasmic reticulum stress induced by PEGylated nanogel containing gold nanoparticles, Cancer Letters. 347 (2014) 151–158. doi:10.1016/j.canlet.2014.02.005.

[9] S. Jain, J.A. Coulter, A.R. Hounsell, K.T. Butterworth, S.J. McMahon, W.B. Hyland, M.F. Muir, G.R. Dickson, K.M. Prise, F.J. Currell, J.M. O'Sullivan, D.G. Hirst, Cell-Specific Radiosensitization by Gold Nanoparticles at Megavoltage Radiation Energies, Int. J. Radiat. Oncol. Biol. Phys. 79 (2) (2011) 531–539. doi:10.1016/j.ijrobp.2010.08.044.

[10] K.T. Butterworth, J.A. Coulter, S. Jain, J. Forker, S.J. McMahon, G. Schettino, K.M. Prise, F.J. Currell, D.G. Hirst, Evaluation of cytotoxicity and radiation enhancement using 1.9 nm gold particles: potential application for cancer therapy, Nanotechnology 21 (2010) 295101. doi:10.1088/0957-4484/21/29/295101.

[11] D.B. Chithrani, S. Jelveh, F. Jalali, M. van Prooijen, C. Allen, R.G. Bristow, R.P. Hill, D.A. Jaffray, Gold Nanoparticles as Radiation Sensitizers in Cancer Therapy, Radiation Research. 173 (2010) 719–728. doi:10.1667/RR1984.1.

[12] T. Kong, J. Zeng, X. Wang, X. Yang, J. Yang, S. McQuarrie, A. McEwan, W. Roa, J. Chen, J.Z. Xing, Enhancement of Radiation Cytotoxicity in Breast-Cancer Cells by Localized Attachment of Gold Nanoparticles, Small 4 (9) (2008) 1537–1543. doi:10.1002/smll.200700794.

[13] C. Wang, Y. Jiang, X. Li, L. Hu, Thioglucose-bound gold nanoparticles increase the radiosensitivity of a triple-negative breast cancer cell line (MDA-MB-231), Breast Cancer 22 (2015) 413–420. doi:10.1007/s12282-013-0496-9.

[14] J. Turkevich, P.C. Stevenson, J. Hillier, A study of the nucleation and growth processes in the synthesis of colloidal gold, Discuss. Faraday Soc. 11 (1951) 55–75.

[15] G. Frens, Controlled nucleation for the regulation of the particle size in monodisperse gold suspensions, Nat. Phys. Sci. 241 (1973) 20−22.

[16] W. Jahnen-Dechent, U. Simon, Function follows form: shape complementarity and nanoparticle toxicity, Nanomedicine 3(5) (2008) 601-603.

[17] R.P. Briñas, M. Hu, L. Qian, E.S. Lymar, J.F. Hainfeld, Gold Nanoparticle Size Controlled by Polymeric Au(I) Thiolate Precursor Size, Journal of the American Chemical Society. 130 (2008) 975–982. doi:10.1021/ja076333e.

[18] C. Zhou, M. Long, Y. Qin, X. Sun, J. Zheng, Luminescent Gold Nanoparticles with Efficient Renal Clearance, Angewandte Chemie International Edition. 50 (2011) 3168–3172. doi:10.1002/anie.201007321.

[19] J. Liu, M. Yu, C. Zhou, S. Yang, X. Ning, J. Zheng, Passive Tumor Targeting of Renal-Clearable Luminescent Gold Nanoparticles: Long Tumor Retention and Fast Normal Tissue Clearance, J. Am. Chem. Soc. 135 (13) (2013) 4978−4981. doi:10.1021/ja401612x.

[20] I. Sondi, O. Siiman, S. Koester, E. Matijević, Preparation of Aminodextran−CdS Nanoparticle Complexes and Biologically Active Antibody−Aminodextran−CdS Nanoparticle Conjugates, Langmuir 16 (2000) 3107–3118. doi:10.1021/la991109r.

[21] B.J. Morrow, E. Matijević, D.V. Goia, Preparation and stabilization of monodisperse colloidal gold by reduction with aminodextran, Journal of Colloid and Interface Science. 335 (2009) 62–69. doi:10.1016/j.jcis.2009.02.053.
[22] S. Jain, D.G. Hirst, J.M. O'Sullivan, Gold nanoparticles as novel agents for cancer therapy, The British Journal of Radiology. 85 (2012) 101–113. doi:10.1259/bjr/59448833.
[23] X.-D. Zhang, J. Chen, Z. Luo, D. Wu, X. Shen, S.-S. Song, Y.-M. Sun, P.-X. Liu, J. Zhao, S. Huo, S. Fan, F. Fan, X.-J. Liang, J. Xie, Enhanced Tumor Accumulation of Sub-2 nm Gold Nanoclusters for Cancer Radiation Therapy, Adv. Healthcare Mater. 3 (2014) 133–141. doi:10.1002/adhm.201300189.
[24] W. Haiss, N.T.K. Thanh, J. Aveyard, D.G. Fernig, Determination of Size and Concentration of Gold Nanoparticles from UV−Vis Spectra, Anal. Chem. 79 (11) (2007) 4215–4221. doi:10.1021/ac0702084.
[25] E.J. Bernhard, A. Maity, R.J. Muschel, W.G. McKenna, Effects of ionizing radiation on cell cycle progression, Radiat. Environ. Biophys. 34 (1995) 79–83.
[26] T.M. Pawlik, K. Keyomarsi, Role of cell cycle in mediating sensitivity to radiotherapy, Int. J. Radiation Oncology Biol. Phys. 59 (4) (2004) 928–942. doi:10.1016/j.ijrobp.2004.03.005.
[27] M.A. Mackey, M.A. El-Sayed, Chemosensitization of Cancer Cells *via* Gold Nanoparticle-Induced Cell Cycle Regulation, Photochem. Photobiol. 90 (2014) 306–312. doi:10.1111/php.12226.
[28] Y. Pan, A. Leifert, D. Ruau, S. Neuss, J. Bornemann, G. Schmid, W. Brandau, U. Simon, W. Jahnen-Dechent, Gold Nanoparticles of Diameter 1.4 nm Trigger Necrosis by Oxidative Stress and Mitochondrial Damage, Small. 5 (2009) 2067–2076. doi:10.1002/smll.200900466.
[29] L. Cui, K. Tse, P. Zahedi, S.M. Harding, G. Zafarana, D.A. Jaffray, R.G. Bristow, C. Allen, Hypoxia and Cellular Localization Influence the Radiosensitizing Effect of Gold Nanoparticles (AuNPs) in Breast Cancer Cells, Radiation Research. 182 (2014) 475–488. doi:10.1667/RR13642.1.
[30] P. Fei, W.S. El-Deiry, P53 and radiation responses, Oncogene 22 (2003) 5774–5783. doi:10.1038/sj.onc.1206677.
[31] W. Roa, X. Zhang, L. Guo, A. Shaw, X. Hu, Y. Xiong, S. Gulavita, S. Patel, X. Sun, J. Chen, R. Moore, J.Z. Xing, Gold nanoparticle sensitize radiotherapy of prostate cancer cells by regulation of the cell cycle, Nanotechnology. 20 (2009) 375101. doi:10.1088/0957-4484/20/37/375101.
[32] J.A. Coulter, S. Jain, K.T. Butterworth, L.E. Taggart, G.R. Dickson, S.J. McMahon, W.B. Hyland, M.F. Muir, C. Trainor, A.R. Hounsell, J.M. O′Sullivan, G. Schettino, F.J. Currell, D.G. Hirst, K.M. Prise, Cell type-dependent uptake, localization, and cytotoxicity of 1.9 nm gold nanoparticles, Int. J. Nanomed. 7 (2012) 2673-2685. doi:10.2147/IJN.S31751.
[33] W. Xu, T. Luo, P. Li, C. Zhou, D. Cui, B. Pang, Q. Ren, S. Fu, RGD-conjugated gold nanorods induce radiosensitization in melanoma cancer cells by downregulating $\alpha_v\beta_3$ expression, International Journal of Nanomedicine. 7 (2012) 915-924. doi:10.2147/IJN.S28314.
[34] N. Chattopadhyay, Z. Cai, Y.L. Kwon, E. Lechtman, J.-P. Pignol, R.M. Reilly, Molecularly targeted gold nanoparticles enhance the radiation response of breast cancer cells and tumor xenografts to X-radiation, Breast Cancer Res. Treat. 137 (2013) 81–91. doi:10.1007/s10549-012-2338-4.

Supplementary material

Syntheses of gold nanoparticles and their impact on the cell cycle of breast cancer cells subjected to megavoltage X-ray irradiation

Nikolina Hanžić[1], Anđela Horvat[1], Juraj Bibić[2], Klaus Unfried[3], Tanja Jurkin[4], Goran Dražić[5], Inga Marijanović[6], Neda Slade[1,*] and Marijan Gotić[7,*]

[1]*Laboratory for Protein Dynamics, Ruđer Bošković Institute, 10002 Zagreb, Croatia*
[2]*University Hospital Center Zagreb, Kišpatićeva 12, 10000 Zagreb, Croatia*
[3]*IUF Leibniz-Institut für Umweltmedizinische Forschung, Auf'm Hennekamp 50, 40225 Düsseldorf, Germany*
[4]*Radiation Chemistry and Dosimetry Laboratory, Ruđer Bošković Institute, 10002 Zagreb, Croatia.*
[5]*National Institute of Chemistry, Hajdrihova 19, SI-1001 Ljubljana, Slovenia*
[6]*Faculty of Science, University of Zagreb, HR 10001 Zagreb, Horvatovac102a, Croatia*
[7]*Center of Excellence for Advanced Materials and Sensing Devices, Ruđer Bošković Institute, 10002 Zagreb, Croatia*

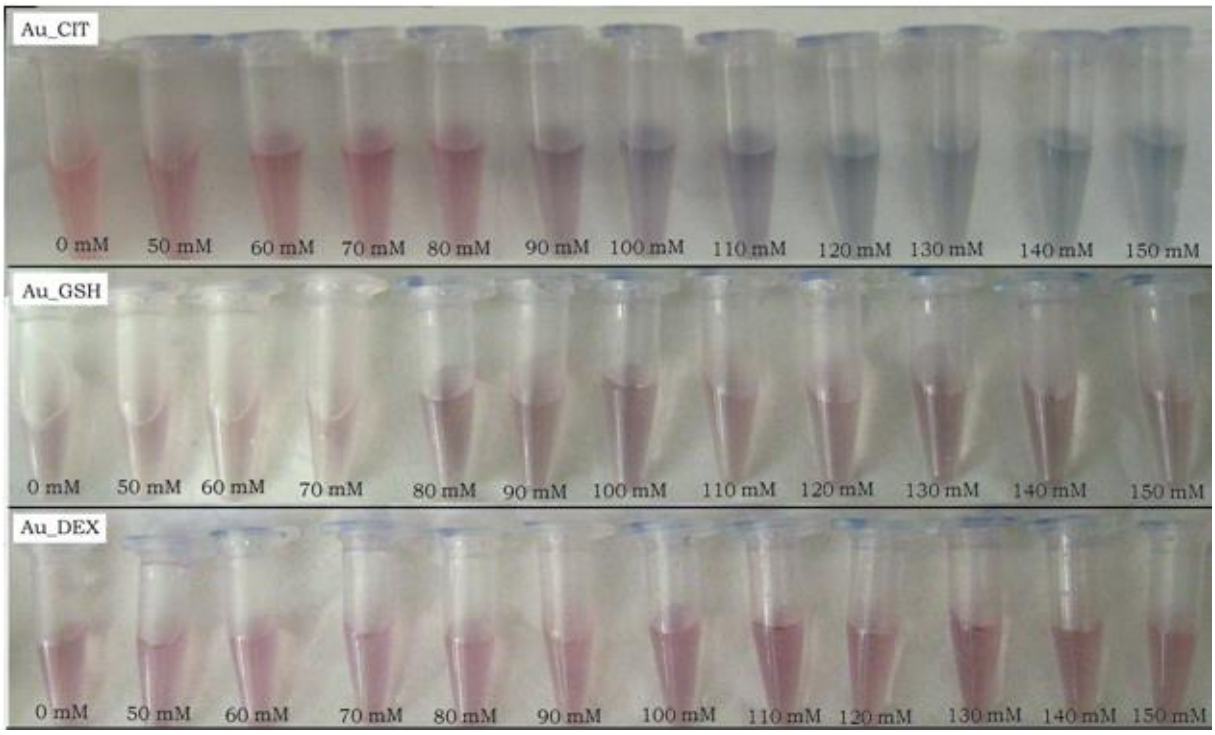

Fig. S1 Investigation of AuNPs salt-induced aggregation. The concentration of NaCl is in the range of 0 to 150 mM. The aggregation of gold nanoparticles in the sample Au-CIT is visible by appearing blue colour at 100 mM NaCl. The intensity of blue colour increases with the increase of NaCl concentration. The samples Au-GSH and Au-DEX are stable against aggregation over the whole range of investigated NaCl concentrations.